ERK promotes tumorigenesis by inhibiting FOXO3a via MDM2-mediated degradation

Jer-Yen Yang[1,2], Cong S. Zong[1], Weiya Xia[1], Hirohito Yamaguchi[1], Qingqing Ding[1], Xiaoming Xie[1], Jing-Yu Lang[1], Chien-Chen Lai[3], Chun-Ju Chang[1], Wei-Chien Huang[1], Hsin Huang[4], Hsu-Ping Kuo[1,2], Dung-Fang Lee[1,2], Long-Yuan Li[3,5], Huang-Chun Lien[6], Xiaoyun Cheng[1,2], King-Jen Chang[7], Chwan-Deng Hsiao[8], Fuu-Jen Tsai[3], Chang-Hai Tsai[3,5], Aysegul A. Sahin[9], William J. Muller[10], Gordon B. Mills[11], Dihua Yu[1,2], Gabriel N. Hortobagyi[12] and Mien-Chie Hung[1,2,3,5,13]

The RAS–ERK pathway is known to play a pivotal role in differentiation, proliferation and tumour progression. Here, we show that ERK downregulates Forkhead box O 3a (FOXO3a) by directly interacting with and phosphorylating FOXO3a at Ser 294, Ser 344 and Ser 425, which consequently promotes cell proliferation and tumorigenesis. The ERK-phosphorylated FOXO3a degrades via an MDM2-mediated ubiquitin-proteasome pathway. However, the non-phosphorylated FOXO3a mutant is resistant to the interaction and degradation by murine double minute 2 (MDM2), thereby resulting in a strong inhibition of cell proliferation and tumorigenicity. Taken together, our study elucidates a novel pathway in cell growth and tumorigenesis through negative regulation of FOXO3a by RAS–ERK and MDM2.

The constitutive activation of certain signal transduction cascades leads to the development of tumours and the resistance of tumours to clinical therapy[1,2]. The RAS–ERK pathway triggers one of these cascades and governs many important functions, such as cell fate, differentiation, proliferation and survival in invertebrate and mammalian cells[3,4]. Human tumours frequently overexpress RAS or harbour activated RAS with a point mutation, which contributes substantially to tumour cell growth, invasion and angiogenesis[1,2,5–8]. Cell plasma membrane receptor tyrosine kinases activate RAS GTPases, and GTP-bound RAS activates A-RAF, B-RAF and RAF-1 (ref. 4), leading to the phosphorylation and activation of the MEK1 and MEK2 pathway. ERK further amplifies the RAS–MEK signalling pathway by targeting different substrates, including transcription factors, kinases and phosphatases, cytoskeletal proteins and apoptotic proteins[3–8]. Recently, ERK and p38 were shown to phosphorylate FOXO1 at various sites[9], suggesting that the RAS–MAPK signalling pathway may play a pivotal role in FOXO regulation.

FOXO transcription factors, one of large forkhead family members, include FOXO1, FOXO3, FOXO4 and FOXO6 (ref. 10). These FOXOs activate or repress multiple target genes involved in tumour

suppression, such as *Bim* and *FasL* for inducing apoptosis[11–13]; *p27kip1* (ref. 14) and *cyclin D*[15] for cell cycle regulation, and *GADD45a* for DNA damage repair[10,11,13,16]. FOXO3a was shown to be associated with tumour suppression activity[17] and inhibition of FOXO3a expression promotes cell transformation, tumour progression and angiogenesis[10,17–19]. More recently, the FOXOs (FOXO1, FOXO3 and FOXO4) knockout mouse has been shown to develop lymphomas and hemangiomas. Thus, the FOXOs function as *bona fide* tumour suppressors[20]. It is known that FOXO3a can be degraded by a ubiquitin-proteasome-dependent pathway[10,17,18,21], but the E3 ubiquitin ligase responsible for FOXO3a degradation has yet to be identified. MDM2, an E3 ubiquitin ligase plays an important role in the development of multiple human cancers through degrading tumour suppressor proteins, such as p53, RB and E-cadherin[22–25]. In addition, MDM2 has been shown to be regulated by the RAS–ERK signalling pathway[26] and blocking ERK activity with an MEK1 inhibitor, U0126, reduces MDM2 expression in breast cancer cells[27].

Here, we identify a novel pathway involving the downregulation of FOXO3a expression by RAS–ERK and MDM2, which leads to promotion of cell growth and tumorigenesis. We show that ERK interacts

[1]Department of Molecular and Cellular Oncology, The University of Texas M. D. Anderson Cancer Center, Houston, TX 77030, USA. [2]Graduate School of Biomedical Sciences, The University of Texas, Houston, TX 77030, USA. [3]China Medical University Hospital, Taichung 404, Taiwan. [4]Department of Internal Medicine, Division of Infectious Diseases, The University of California, Davis, CA 95817, USA. [5]Asian University, Taichung 413, Taiwan. [6]Department of Pathology and [7]Department of Surgery, College of Medicine, and Angiogenesis Research Center, National Taiwan University, Taipei 106, Taiwan. [8]Institute of Molecular Biology, Academia Sinica, Taipei 115, Taiwan. [9]Department of Pathology, The University of Texas M. D. Anderson Cancer Center, Houston, TX 77030, USA. [10]Departments of Medicine and Biochemistry, McGill University, Montreal, Quebec, H3A 1A1, Canada. [11]Department of Systems Biology, The University of Texas M. D. Anderson Cancer Center, Houston, TX 77030, USA. [12]Department of Breast Medical Oncology, The University of Texas M. D. Anderson Cancer Center, Houston, TX 77030, USA. [13]Correspondence should be addressed to M.-C.H. (e-mail: mhung@mdanderson.org)

Figure 1 ERK suppresses FOXO3a stability and induces its nuclear exclusion. (a–d) Lysates of 293T cells were subjected to immunoblotting with the indicated antibodies after being transfected with ERK2 and MEK1^{CA} (a), control vector or ERK^{DN} (b), ERK2^{DN} and MEK1^{CA} (c), and control vector and *ERK1* and *ERK2* siRNA (d). (e–h) Lysates of the following cells were analysed by direct immunoblotting with the indicated antibodies: MDA-MB-453 cells were treated with DMSO or U0126 (2 µM) for 4 h (e), NIH3T3 cells and NIH3T3 RAS-transformed cells (f), Hep-3B and Hep-3BX (g), and Hep-3BX (h) cells were treated with increasing dosages of U0126. (i) MCF-7 cells were extracted at the indicated times after CHX (1 µg ml⁻¹) incubation before treatment with either DMSO (control) or U0126. (j–l) Lysates of MCF-7 cells (j) treated with (DMSO, U0126, or PD98059 (20 µM)), NIH3T3 and NIH3T3 VRAS-transformed cells (k), and Hep-3B and Hep-3BX cells (l) were subjected to immunoblotting with the indicated antibodies. (m) Real-time PCR transcript of *p27Kip1* and *Bim* were measured, and the relative fold of induction was calculated and compared between DMSO or U0126 treated cells. (n) Lysates of 293T cells cotransfected with control vectors were subjected to luciferase assays with a *p27* promoter-driven luciferase reporter. In m and n, representative results s.d. from three experiments (*n* = 3) conducted in duplicates are shown. (o) Hep-3B cells were serum starved and then treated with EGF (50 ng ml⁻¹) for 30 min in the presence (+) or absence (–) of U0126. Nuclear and cytoplasmic fractions were then analysed by immunoblotting with the indicated antibodies. Equal amount of lysates was loaded in each lane. Similar results were also obtained by using MCF-7 cells (data not shown). Uncropped images of the scans in a, h, i and k are shown in the Supplementary Information, Fig. S5.

with and phosphorylates FOXO3a at Ser 294, Ser 344 and Ser 425; phosphorylation of FOXO3a at these residues increases FOXO3a–MDM2 interaction and enhances FOXO3a degradation via an MDM2-dependent ubiquitin-proteasome pathway. The non-phosphorylated

FOXO3a-mimic mutant, compared to the phosphorylated FOXO3a-mimic mutant, exhibits more resistance to the interaction and degradation by MDM2, resulting in a strong inhibition of cell proliferation *in vitro* and tumorigenesis *in vivo*.

Table 1 Inverse correlation between MDM2 and FOXO3a expression in human breast cancer tissues			
FOXO3a	MDM2		Total
	–	+	
–	17 (21.6)	61 (48.8)	78 (62.4)
+	20 (16.0)	27 (13.6)	47 (37.6)
Total (percentage)	37 (29.6)	88 (70.4)	125 (100)

The 125 surgical breast cancer tumour specimens were analysed by immunohistochemical staining antibodies specific to FOXO3a and MDM2, respectively. The expression pattern of FOXO3a and MDM2 was analysed by using χ-square test ($P = 0.0138$). A P value of less than 0.05 was considered statistically significant.

RESULTS

ERK suppresses FOXO3a stability and induces its nuclear exclusion

The RAS–ERK is an essential oncogenic signalling cascade that promotes tumour cell growth and development[8,28]. It was known that other oncogenic kinases, AKT and IKK, negatively regulate FOXO3a. In an attempt to understand the molecular mechanisms that trigger cell growth and tumour development, we asked whether ERK could regulate FOXO3a expression. When a constitutively active MEK1 (MEK1[CA]) that activated ERK was transfected into 293 cells, the total FOXO3a protein was reduced (Fig. 1a). Furthermore, dominant-negative ERK (ERK[DN]) rescued FOXO3a expression suppressed by MEK1[CA] (Fig. 1b, c). Similarly, using *ERK* small interference RNA (siRNA) to knockdown ERK protein expression level in HeLa cells (Fig. 1d), or treatment with U0126, a MEK1 inhibitor (Fig. 1e) led to a dose-dependent increase in FOXO3a protein expression (see Supplementary Information, Fig. S1a). At the same time, *FOXO3a* RNA levels were only slightly increased in response to U0126 (see Supplementary Information, Fig. S1b). Taken together, the results indicate that ERK mainly downregulates FOXO3a protein expression.

To validate the observation that ERK mediated the downregulation of FOXO3a, two cell lines with elevated ERK activities were used[29], NIH3T3-V12Ras and Hep-3BX (a human hepatoma-derived cell line). Both cell lines showed pronounced decrease of FOXO3a protein compared to the wild-type parental cell lines (Fig. 1f, g), and treatment with U0126 increased FOXO3a protein levels in a dose-dependent manner (Fig. 1h). Similarly, a reduction in FOXO3a expression was observed with both EGF and 12-O-tetradecanoylphorbol 13-acetate (TPA) treatment, both of which activate ERK. The increased FOXO3a expression was restored by inhibition of ERK activity (see Supplementary Information, Fig. S1c, d). To determine whether the ERK-mediated downregulation of FOXO3a protein expression was due to effects on FOXO3a stability, the half-life of FOXO3a protein was examined when treated with U0126. FOXO3a protein levels were significantly reduced after approximately 2 h, but remained stable for 7 h when treated with the the MEK inhibitor, U0126 (Fig. 1i). Moreover, the half-life of FOXO3a was approximately 6 h in 293 cells, as determined by ^{35}S-methionine pulse-chase labelling experiments. However, in the presence of U0126, FOXO3a lasted more than 8 h (see Supplementary Information, Fig. S1e). The data indicate that ERK regulates FOXO3a by reducing FOXO3a stability.

To determine whether this regulation could exert an effect on downstream targets of FOXO3a (such as *p27Kip1* and *Bim*), expression levels were measured and FOXO3a, p27kip1 and Bim proteins were shown to be increased in cells treated with MEK1 inhibitors, U0126 or PD98059 (Fig. 1j), whereas levels of these proteins were suppressed in the ERK-activated NIH3T3-V12Ras and Hep-3BX cell lines compared to the parental cells lines (Fig. 1k, l). Furthermore,

both *Bim* and *p27kip1* RNAs, known to be transcriptionally regulated by FOXO3a, were increased in the presence of U0126, as shown by real time RT–PCR (Fig. 1m). MEK1[CA] expression significantly inhibited *p27* promoter-driven luciferase reporter expression (Fig. 1n), as well as FOXO3a-dependent transcriptional activation of pGL2-6xBDB (a luciferase reporter containing FOXO-responsive elements) in a dose-dependent manner (see Supplementary Information, Fig. S1f). Taken together, the results suggest that ERK inhibits *p27Kip1* and *Bim* transcription by downregulating FOXO3a.

It is known that AKT and IKK oncogenic kinases regulate FOXO3a nuclear exportation through direct phosphorylation at Ser 253 and Ser 644, respectively[17,30]. We asked whether phosphorylation of FOXO3a by ERK could also lead to nuclear exclusion. To this end, nuclear and cytoplasmic fractionation was performed to determine whether FOXO3a subcellular distribution was regulated by ERK (Fig. 1o). ERK activation was induced by treatment with EGF for 30 min, either in the presence or absence of MEK1 inhibitor, U0126. FOXO3a levels were reduced in the nucleus but increased in the cytoplasm with EGF treatment, suggesting that FOXO3a was translocated from the nucleus to the cytoplasm. As expected, p-FOXO3a was increased in the cytoplasm with ERK activation and decreased with ERK inhibition (Fig. 1o). Non-phosphorylated FOXO3a levels were also slightly increased in the nucleus after 30 min treatment with U0126 (Fig. 1o), and the increase became more obvious with a 2 h U0126 treatment (see Supplementary Information, Fig. S2e). Taken together, the results suggest ERK-phosphorylated FOXO3a may translocate from nucleus to cytoplasm and lose its transcriptional activity.

ERK interacts with and phosphorylates FOXO3a predominantly on Ser 294, Ser 344 and Ser 425

To explore the mechanism of ERK-mediated FOXO3a downregulation, the interaction between ERK and FOXO3a was characterized. Both endogenous and exogenous FOXO3a physically associated with endogenous and exogenous ERK (Fig. 2a, b). Immunoblot probing of FOXO3a revealed a remarkable band shift 10 min after treatment with EGF, which then shifted back to basal levels after 4 h. This band-shifted pattern correlated with p-ERK (see Supplementary Information, Fig. S2f) and was blocked by U0126 (see Supplementary Information, Fig. S2g), suggesting that FOXO3a was post-translationally modified in the presence of p-ERK. The FOXO3a band shift after EGF stimulation also shifted back to basal line after treatment with calf intestinal alkaline phosphatase (CIP), further indicating that the post-translational modification of FOXO3a was due to phosphorylation, presumably by p-ERK (Fig. 2c).

To further determine whether ERK could directly phosphorylate FOXO3a, an *in vitro* kinase assay was performed, and revealed that full-length FOXO3a–GST fusion proteins were phosphorylated by recombinant-activated ERK proteins directly (see Supplementary Information,
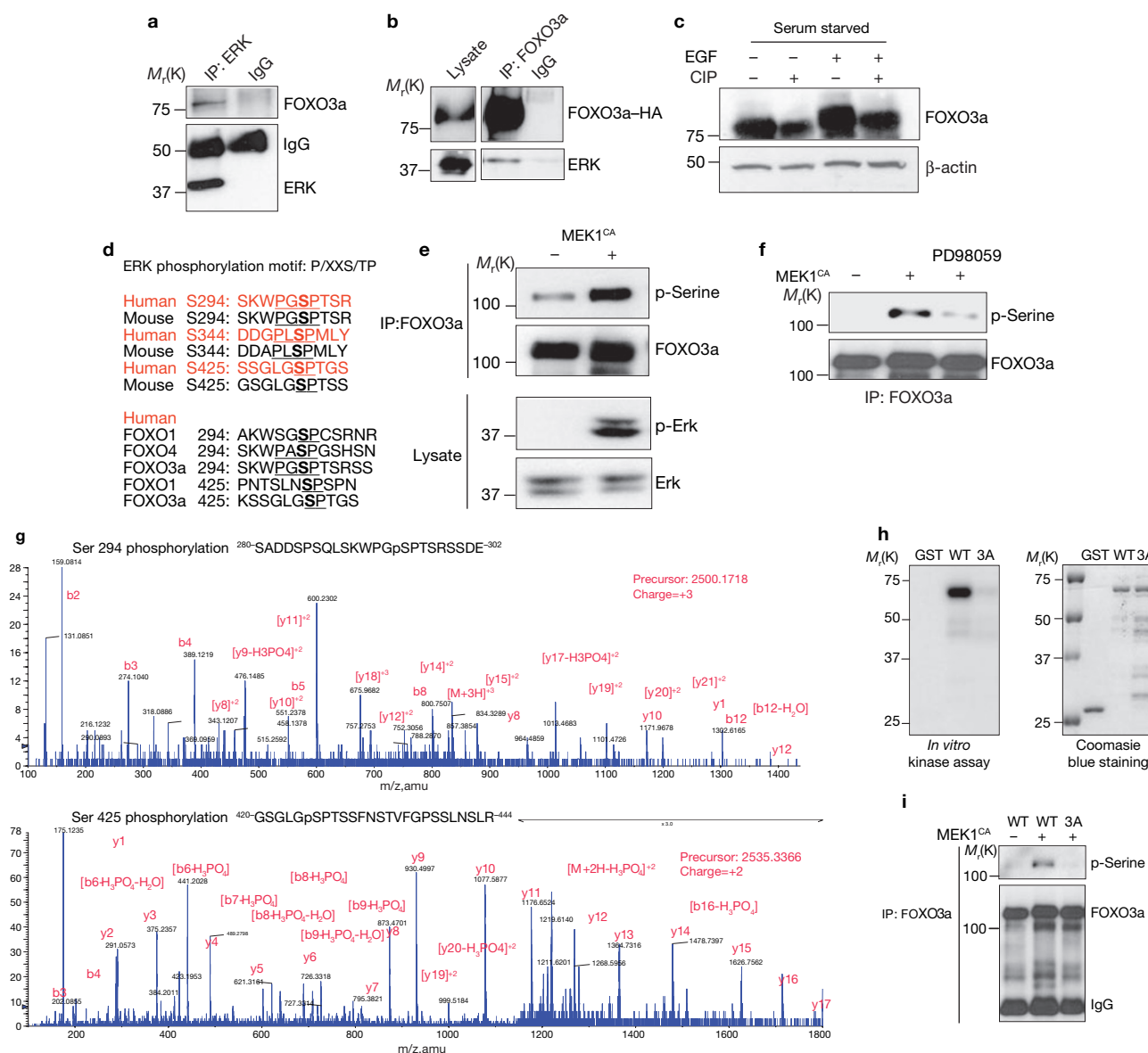
Figure 2 ERK interacts with and phosphorylates FOXO3a *in vitro* and *in vivo*. (**a**) Lysates of MCF-7 cells were subjected to immunoprecipitation and immunoblotting with anti-ERK and anti-FOXO3 antibodies, respectively. (**b**) Lysates of 293T cells transfected with FOXO3a–HA and ERK were subjected to immunoprecipitation with an anti-HA antibody and immunoblotting with an anti-ERK antibody. (**c**) The lysates from MCF-7 cells serum starved overnight and stimulated with EGF for 30 min were treated with CIP and subjected to immunoblotting. (**d**) The putative ERK consensus sequences for phosphorylation on FOXO3a were: P, proline; S, serine; T, threonine; and X, any amino acid. (**e**) Lysates of 293T cells transfected with GFP–FOXO3a and control or MEK1^{CA} plasmids were subjected to immunoprecipitation with an anti-FOXO3a antibody and immunoblotting with an anti-phospho-serine antibody

or direct immunoblotting with either an anti-p-ERK or an anti-ERK antibody. (**f**) Cells treated with PD98059 for 4 h before the lysates were extracted and subjected to analysis as described in **e**. (**g**) Lysates from MCF-7 cells that had been serum starved overnight and stimulated with EGF for 30 min were subjected to immunoprecipitation with an anti-FOXO3a antibody, and the isolated FOXO3a bands were subjected to mass spectrometry. (**h**) *In vitro* kinase assays were conducted by incubating recombinant activated ERK2 with GST–FOXO3a (281–673) and mutant GST–FOXO3a^{3A} proteins. (**i**) Lysates of 293T cells cotransfected with FOXO3a or mutant FOXO3a^{3A} and MEK1^{CA} were subjected to immunoprecipitation with an anti-FOXO3a antibody and immunoblotting with an anti-phospho-serine antibody. An uncropped image of the blot is shown in the Supplementary Information, Fig. S5

Fig. S2h). By isolating phosphorylated FOXO3a from the *in vitro* kinase assay (data not shown) and analysing it by mass spectrometry, three ERK-specific phosphorylation sites were identified in FOXO3a: Ser 294, Ser 344 and Ser 425. A BLAST search of the National Center for Biotechnology Information database revealed that Ser 294, Ser 344 and Ser 425 of FOXO3a are common residues in other FOXO subfamily members, and are conserved in both humans and mice (Fig. 2d).

To confirm that all three of these ERK-specific phosphorylation sites existed in FOXO3a *in vivo*, an anti-phospho-serine antibody was used to detect serine-phosphorylated FOXO3a in MEK1^{CA}-transfected cells (Fig. 2e). The serine phosphorylation of FOXO3a was abolished by MEK1 inhibitor (PD98059) treatment (Fig. 2f). Phosphorylation of Ser 294 and Ser 425 was identified by *in vivo* mass spectrometry from MCF-7-cell extracts (Fig. 2g). Phosphorylation of Ser 344 was not

Combined	Tumour grade		Total
	Low	High	
MDM2– FOXO3a–	0 (0.0)	17 (16.50)	17
MDM2+ FOXO3a–	9 (40.91)	52 (50.49)	61
MDM2– FOXO3a+	7 (31.82)	13 (12.62)	20
MDM2+ FOXO3a+	6 (27.27)	21 (20.39)	27
Total	22	103	125

Table 2 MDM2+ and FOXO3a– is associated with higher tumour grade in breast cancer patients.

The relationship between combined expression of FOXO3a and MDM2 and tumour grade in human breast cancer specimens was analysed using a χ-square test. A P value of <0.05 was considered statistically significant.

detected in the mass spectrometry analysis, but was confirmed using a newly developed antibody that can recognize phospho-Ser 344 of FOXO3a, and the phosphorylated FOXO3a was mainly located in the cytoplasm when p-ERK was activated by EGF treatment (Fig. 1o and see Supplementary Information, Fig. S2a–c). The original intention was to generate phospho-specific antibodies against all three phospho-serine peptides of FOXO3a. However, only two phospho-specific antibodies were successful, those against p-Ser 344 and p-Ser 425 (see Supplementary Information, Fig. S2d). These two phospho-specific antibodies were further used to demonstrate that MEK1^{CA} stimulates phosphorylation of Ser 344 and Ser 425 (see Supplementary Information, Fig. S2d).

FOXO3a^{3A}, a mutant in which all three serine residues were substituted for alanine residues to mimic a non-phosphorylated status, was resistant to phosphorylation by ERK in kinase assays *in vitro* compared with wild-type FOXO3a (Fig. 2h). Consistent with the *in vitro* kinase assay data, FOXO3a^{3A} had a significantly lower serine phosphorylation levels *in vivo* than wild-type FOXO3a (Fig. 2i). Taken together, the data support that the three serine residues are specific phosphorylation sites for ERK.

MDM2 is required for ERK-mediated FOXO3a degradation

As the RAS–ERK pathway was known to upregulate MDM2 protein expression[26,27], and ERK was shown to downregulate FOXO3a protein expression and stability in our experiments (Fig. 1a–h and i), we further asked whether MDM2 might be involved in the ERK-mediated FOXO3a downregulation. First, endogenous MDM2 was shown to associate with FOXO3a in MCF-7 cells by reciprocal immunoprecipitation (Fig. 3a). MDM2 also reduced endogenous FOXO3a protein levels in a dose-dependent manner (Fig. 3b) and the reduced FOXO3a levels were recovered when treated with the proteasome inhibitor MG-132 (Fig. 3c), which suggests that FOXO3a stability was regulated through proteasome degradation. In addition, a FOXO3a protein gel exhibited a polyubiquitination pattern when ubiquitin was coexpressed, suggesting that FOXO3a was subjected to polyubiquitin modification and further proteasomal degradation (Fig. 3c). Consistently, *p53*$^{–/–}$*MDM2*$^{–/–}$ double-knockout MEFs showed more stabilized FOXO3a expression compared with *p53*$^{–/–}$ MEF cells (Fig. 3d). Taken together, these results indicate that MDM2 associates with FOXO3a and may function as an ubiquitin ligase for FOXO3a proteasomal degradation.

To further determine the pathological relevance of the relationship between MDM2 and FOXO3a expression, we examined whether the expression of MDM2 might be inversely correlated with FOXO3a expression in human breast cancer tissues. A significant correlation between the MDM2-positive and FOXO3a-negative tissues was found in a cohort of 125 breast cancer patients (Table 1). Representative tumours from

consecutive sections of six different patients stained with FOXO3a and MDM2 are shown in the Supplementary Information, Fig. S3a. To support the reliability of immunohistochemical staining, fourteen freshly prepared human breast tumour lysates were immunoblotted. Both the immunohistochemical staining and immunoblotting showed a reverse correlation between FOXO3a and MDM2 expression (see Supplementary Information Fig. S3b). In addition, the MDM2-positive and FOXO3a-negative expression pattern was also significantly associated with higher tumour grade (Table 2). Thus, MDM2-mediated downregulation of FOXO3a may play a role in the development of human breast cancer.

We then asked whether MDM2 was required for ERK-mediated FOXO3a donwnregulation. In *p53*$^{–/–}$ MEFs, FOXO3a protein levels were stabilized by MEK1 inhibitors (U0126, PD98059), which stabilized FOXO3a level similar to the extent as the proteasome inhibitor MG-132 (Fig. 3e). Examining the cell line, *p53*$^{–/–}$*MDM2*$^{–/–}$ MEFs, showed that FOXO3a protein levels were not affected by ERK inhibition in the absence of MDM2 (Fig. 3e), which further indicated that ERK regulation of FOXO3a stability is MDM2 dependent. FOXO3a half-life was further examined by employing the protein synthesis inhibitor cycloheximide (CHX) and with pulse-chase experiments using ^{35}S-methionine labelling. In *p53*$^{–/–}$ MEFs, FOXO3a protein levels decrease 50% after 4 h treatment with CHX and, consistently, in pulse-chase experiments, FOXO3a protein levels were also decreased 50% in approximately 6 h (Fig. 3f, h). However, in *p53*$^{–/–}$*MDM2*$^{–/–}$ MEFs, FOXO3a expression remained constant, even after 8 h CHX treatment and 10 h ^{35}S-methionine labelling analysis (Fig. 3g, h), indicating that MDM2 is required for downregulation of FOXO3a. Taken together, the results suggest that MDM2 mediates ERK-mediated FOXO3a degradation.

MDM2 degrades FOXO3a^{3D} via the ubiquitin-proteasome degradation pathway

To further support the evidence that the ERK-mediated phosphorylation of FOXO3a alters its stability, the stability of two mutant proteins was compared: FOXO3a^{3A}, a non-phosphorylation-mimic mutant, and FOXO3a^{3D}, a phosphorylation-mimic mutant. FOXO3a^{3D} levels decreased after 2 h CHX treatment and the downregulation was rescued by the addition of MG-132 (Fig. 4a). In comparison, FOXO3a^{3A} levels remained unchanged in the presence of CHX for more than 8 h (Fig. 4a), and were similar to the levels in FOXO3a^{3D}-expressing cells that had been treated with MG-132 (Fig. 4a). Together with the data shown in Fig. 1i, the results suggest that phosphoryaltion of FOXO3a by ERK regulates FOXO3a protein stability.

Next, we examined the role of ERK in MDM2-mediated FOXO3a degradation. To determine whether ERK status affects the association between MDM2 and FOXO3a, the association between endogenous and
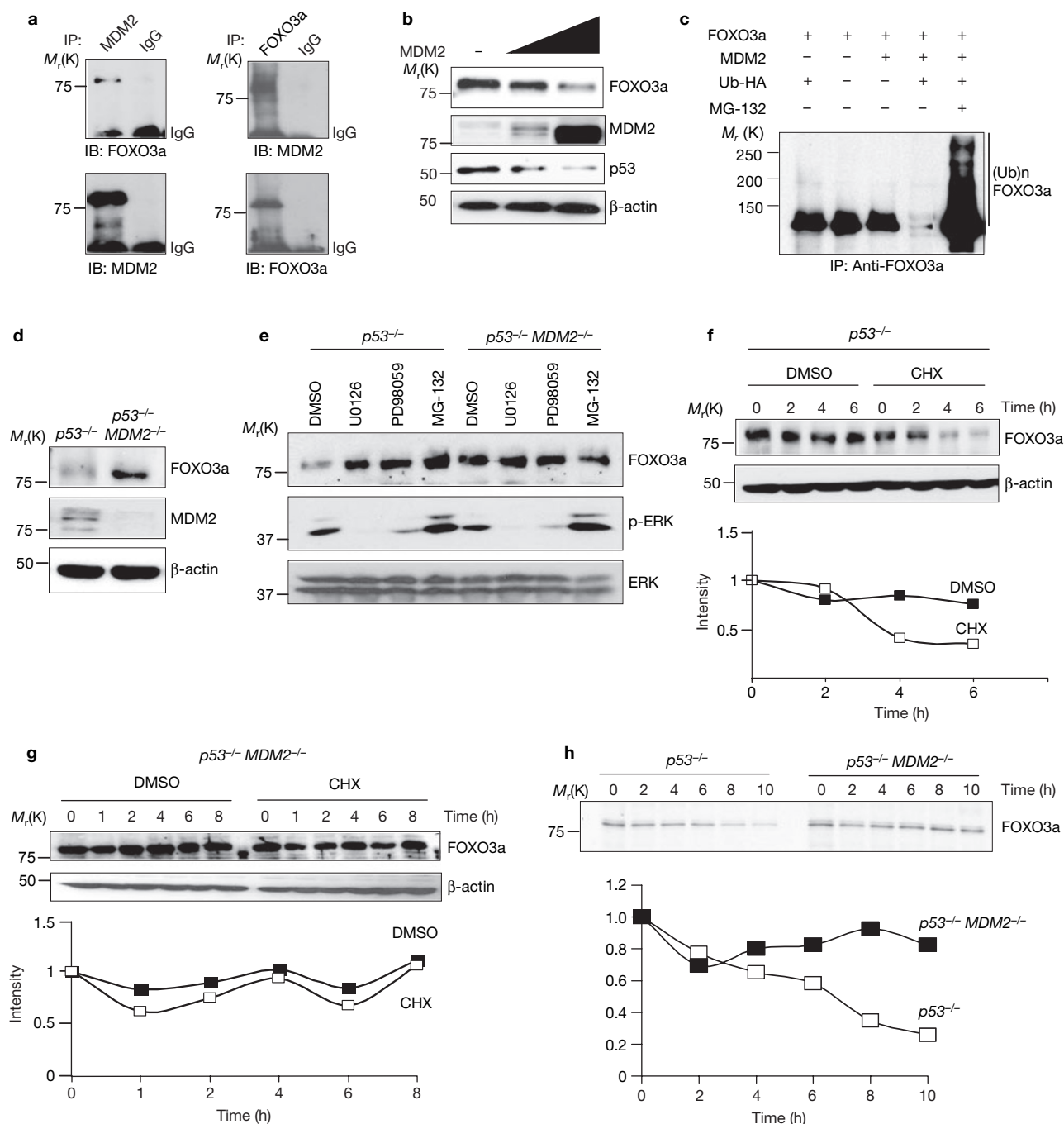
Figure 3 MDM2 is required for ERK-mediated FOXO3a degradation. (**a**) MCF-7 cell lysates were subjected to immunoprecipitation with an anti-MDM2 antibody and immunoblotting with an anti-FOXO3a antibody. (**b**) Lysates of 293T cells transfected with MDM2 at different dosages and subjected to immunoblotting. (**c**) Lysates of cotransfected cells treated with the indicated vectors in the presence of MG-132 (20 μM, 4 h) were subjected to immunoprecipitation and immunoblotting with an anti-FOXO3a antibody. (**d**) Lysates of $p53^{-/-}$ or $p53^{-/-}MDM^{-/-}$ MEFs were subjected to immunoblotting using different antibodies, as indicated. (**e**) MEFs were treated with different inhibitors and analysed by immunoblotting. (**f**, **g**) MEFs were treated with or without CHX, harvested at the indicated times and subjected to immunoblotting. (**h**) MEFs were treated with methionine and cysteine-free medium overnight, pulsed with ^{35}S-Met-Cys for 30 min, and chased for the indicated times. Cell lysates were immunoprecipitated with an anti-FOXO3a antibody and subjected to SDS–PAGE, gels were fixed, dried, and subjected to autoradiography (with an intensifying screen). An uncropped image of the blot in **e** is shown in the Supplementary Information, Fig.S5.

exogenous MDM2 and FOXO3a was examined, and was enhanced in EGF-stimulated cells, but was reduced with U0126 treatment (Fig. 4b, c). Consistently, the FOXO3a^{3D} mutant mimicking ERK-phosphorylated FOXO3a interacted more strongly with MDM2 than the FOXO3a^{3A}

mutant mimicking non-phosphorylated FOXO3a (Fig. 4d). These results suggest that ERK-induced phosphorylation of FOXO3a mediates MDM2-dependent degradation and may serve as a docking site for MDM2 to bind with and ubiquitinate FOXO3a for further degradation.
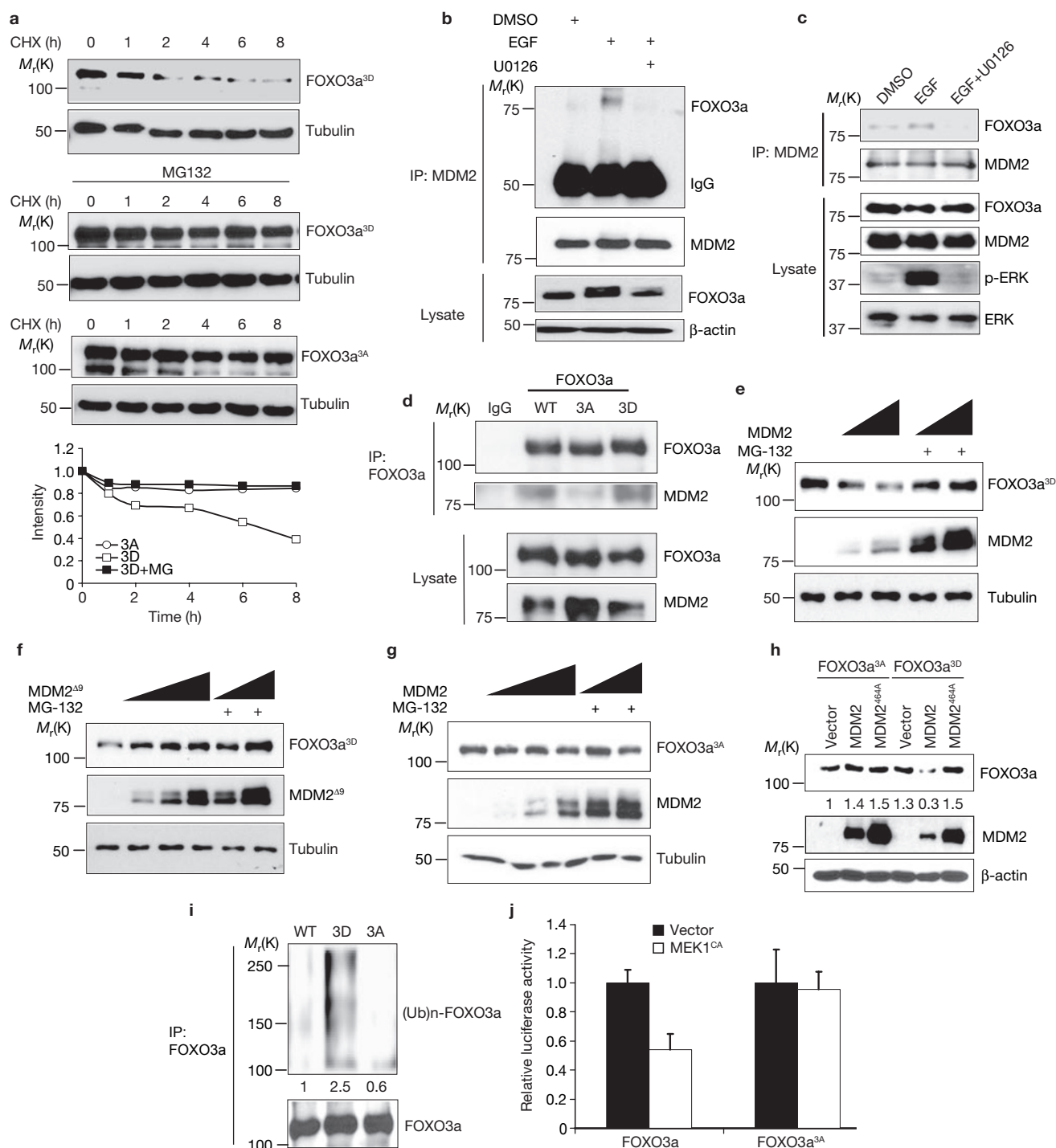
Figure 4 Phosphorylation of FOXO3a by ERK facilitates MDM2-mediated FOXO3a degradation through an ubiquitin-proteasome pathway. (**a**) Lysates of 293T cells transfected with GFP–FOXO3a^{3A} or GFP–FOXO3a^{3D} were harvested at different time points after treated with CHX or MG-132 were analysed by immunoblotting. (**b**) Lysates of MCF-7 cells were subjected to immunoprecipitation and immunoblotting under different conditions. (**c**, **d**) Lysates of 293T cells transfected with wild-type (WT) FOXO3a (**c**) and 293T cells transfected with wild-type FOXO3a or mutants FOXO3a^{3A} and FOXO3a^{3D} (**d**) were subjected to immunoprecipitation and immunoblotting. (**e**–**g**) Lysates of 293T cells cotransfected with FOXO3a^{3D} (**e**) or FOXO3a^{3A} (**g**), together with different dosages of wild-type MDM2 or deletion mutant of MDM2, MDM2^{Δ9} (**f**), with or without MG-132, were analysed by immunoblotting. (**h**) Lysates of 293T cells cotransfected with FOXO3a^{3A} or FOXO3a^{3D}, together with wild-type MDM2 or mutant MDM2^{464A} were subjected to immunoblotting. (**i**) Lysates of 293T cells cotransfected with wild-type FOXO3a, FOXO3a^{3D} or FOXO3a^{3A}, together with MDM2 and ubiquitin in the presence of MG-132, were analysed by immunoblotting. (**j**) Lysates of 293T cells cotransfected with 6XDBE–Luc and pRL-TK, and FOXO3a or FOXO3a^{3A}, together with control vector or MEK1^{CA} were subjected to luciferase assay. The results were from three experiments ($n = 3$) with the error bars representing s.d. from duplicates in each case. Uncropped images of the blots in **e**–**g** are shown in the Supplementary Information, Fig. S6.
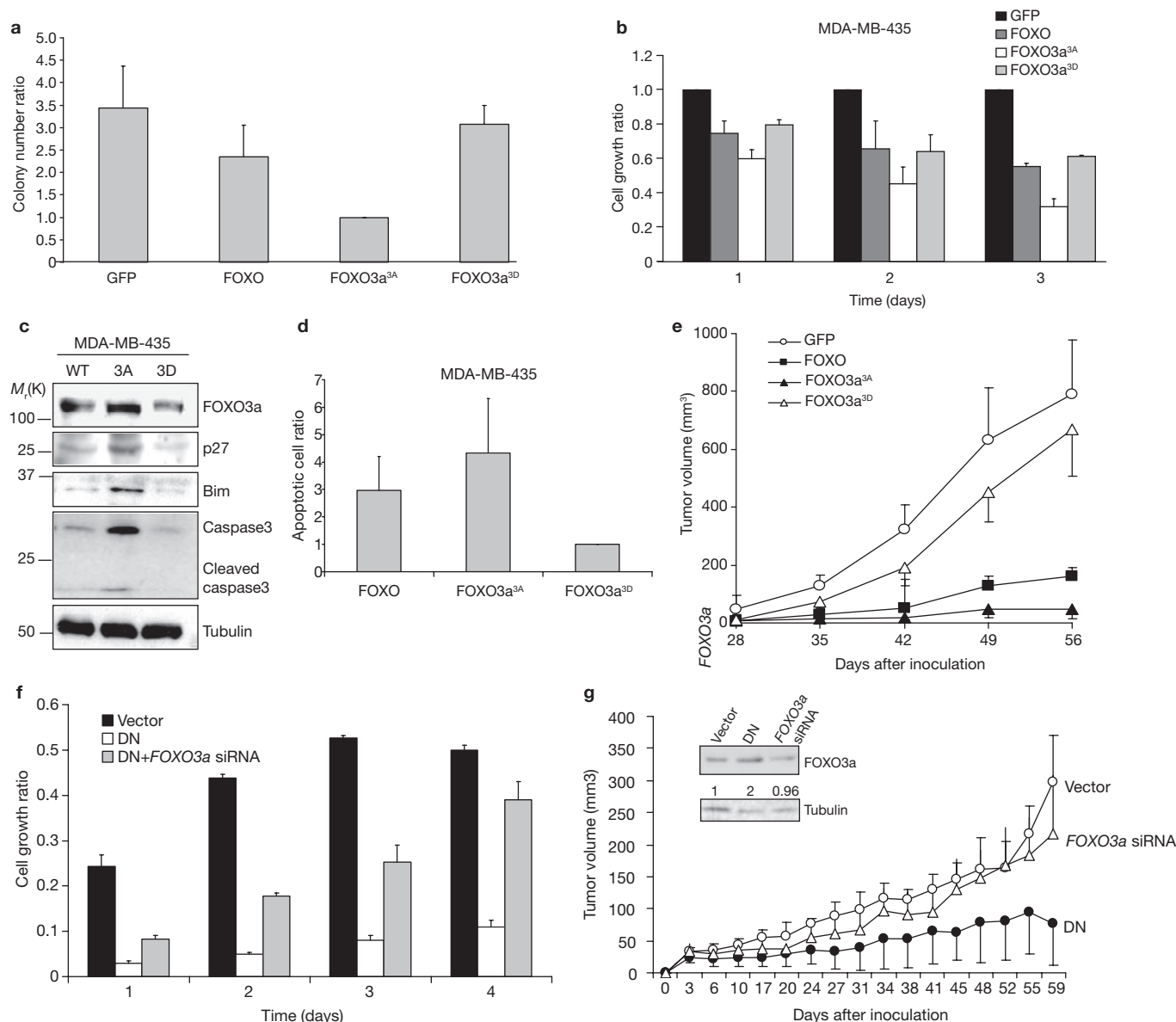
Figure 5 FOXO3a[3A], but not FOXO3a[3D], inhibits tumorigenesis and induces apoptosis. (**a**) MDA-MB-435 cells were transfected with control vector, wild-type FOXO3a, FOXO3a[3A] or FOXO3a[3D]. After sorting with GFP marker, GFP-positive cells were subjected to the colony formation and MTT assays. (**b**) Cells obtained as described in **a** were measured for cell growth rate by MTT assay. All experiments were performed in triplicate (*n* = 3). A representative sample is shown in **a** and **b**. (**c**) Lysates from cells obtained as described in **a** and MDA-MB-435 cell lines, as indicated, were analysed by immunoblotting. (**d**) MDA-MB-435 cells were transfected with control vector, wild-type FOXO3a, FOXO3a[3A] or FOXO3a[3D] and, after propidium iodide (PI) staining, the cells were analysed by FACS, performed as described in the

Methods. Only the GFP-positive cells were measured in the sub-G1 phase as apoptotic cells, and the apoptosis ratio was normalized with the control vector. (**e**) The MDA-MB-435-transfected cell lines were sorted for GFP-positive cells, which then were injected into the mammary fat pads of nude mice. (**f**) MDA-MB-435 cells were transfected with control vector, ERK1[DN] and ERK2[DN] (DN), and ERK1[DN], ERK2[DN] and *FOXO3a* siRNA, and the cells were subjected to MTT assays. (**g**) Cells (2 × 10^6) cells obtained as described in **f** were injected into the mammary fat pads of nude mice. The tumour volume was measured twice per week. The inset shows FOXO3a expression quantified by normalization with tubulin expression. An uncroppped image of the blot in **c** is shown in the Supplementary Information, Fig. S6.

To determine whether the interaction between p-FOXO3a and MDM2 promotes FOXO3a degradation, FOXO3a[3D] and MDM2 were cotransfected in 293T cells. As expected, FOXO3a[3D] levels were inversely correlated with MDM2 protein levels, and MG-132 treatment stabilized FOXO3a[3D] levels (Fig. 4e). FOXO3a[3D] levels remained unchanged in the presence of either MDM2[Δ9] or MDM2[464A] mutants known to dramatically reduce the ubiquitin ligase activity of MDM2 (refs 31–33; Fig. 4f, h), but decreased approximately fourfold in the presence of wild-type

MDM2 (Fig. 4e, h). In addition, FOXO3a[3A] levels were not affected by the presence of wild-type MDM2 (Fig. 4g, h) suggesting that the FOXO3a[3D] mutant is more susceptible to degradation by MDM2 than FOXO3a[3A].

Ubiquitination of the wild-type and mutant FOXO3a was then examined. FOXO3a[3D] was heavily ubiquitinated, whereas FOXO3a[3A] was resistant to polyubiquitination (Fig. 4i). FOXO3a[3A] mutant was also resistant to MEK1[CA]-mediated inactivation of FOXO3a transcriptional activity, as measured by a luciferase reporter assay (Fig. 4j). Taken together, the data

show that MDM2 may serve as an E3 ligase for FOXO3a degradation, and that the interaction between MDM2 and FOXO3a is dependent on ERK kinase activity through phosphorylating FOXO3a, thus making it more susceptible to MDM2-mediated degradation.

FOXO3a³ᴬ inhibits tumorigenesis and induces apoptosis

We further examined the function of FOXO3a³ᴬ and FOXO3a³ᴰ in cell transformation and tumorigenesis by introducing vector–GFP, wild-type FOXO3a–GFP, FOXO3a³ᴬ–GFP and FOXO3a³ᴰ–GFP expression vectors into MDA-MB-435 breast cancer cells. GFP-positive cells were sorted and selected for soft agar colony formation assays and MTT cell proliferation assays. Wild-type FOXO3a decreased colony formation by 23% compared to GFP alone. FOXO3a³ᴬ–GFP inhibited colony formation by 70%, whereas FOXO3a³ᴰ–GFP led to an 11% inhibition (Fig. 5a). FOXO3a³ᴬ–GFP also exhibited more potent inhibition activity in the MTT cell proliferation assays (Fig. 5b and see Supplementary Information, Fig. S4a).

Notably, p27, Bim and cleaved-caspase3 proteins were upregulated in FOXO3a³ᴬ cells, but not in FOXO3a³ᴰ cells (Fig. 5c), suggesting that cell-cycle regulation and apoptosis contribute to the anti-proliferative activity of FOXO3a³ᴬ (Fig 5c). As shown in Fig. 5d, cells transfected with FOXO3a³ᴬ–GFP exhibitd fourfold more apoptosis than those transfected with FOXO3a³ᴰ–GFP. To further test the tumour suppression activity *in vivo*, GFP-positive cells were inoculated into the mammary fat pads of nude mice, which were then monitored for tumour development (Fig. 5e). FOXO3a³ᴬ inhibited tumour growth, whereas the FOXO3a³ᴰ mutant had no tumour-suppression activity. Our results suggest that non-phosphorylated form of FOXO3a is a stronger suppressor of tumorigenesis than its phosphorylated counterpart, and that the phosphorylation and downregulation of FOXO3a facilitate its tumour suppression activity.

To further determine whether ERK promotes tumorigenesis through downregulation of FOXO3a, MDA-MB-435 breast cancer cells were transfected with ERKᴰᴺ or ERKᴰᴺ along with *FOXO3a* siRNA. In MTT assays, ERKᴰᴺ reduced breast cancer cell growth, which was restored by treatment with *FOXO3a* siRNA (Fig. 5f). The *FOXO3a* siRNA result was validated by rescuing its effects with FOXO3a overexpression (see Supplementary Information, Fig. S4b, 4c). Furthermore, ERKᴰᴺ strongly inhibited tumour growth in animals, and ERKᴰᴺ-mediated tumour suppression required expression of FOXO3a, as treatment with *FOXO3a* siRNA reduced its tumour suppression activity (Fig. 5g). Taken together, the results suggest that ERK may enhance tumorigenecity by downregulation of FOXO3a.

DISCUSSION

Here, we propose a novel signalling pathway: the tumour suppressor gene *FOXO3a* is regulated by the oncoprotein ERK through interaction and degradation by the MDM2-mediated ubiquitin-proteosome pathway (Fig. 6). We identified three FOXO3a Erk kinase phosphorylation sites (Ser 294, Ser 344 and Ser 425). Phosphorylation of these serine residues increases FOXO3a cytoplasmic distribution and susceptibility to interaction and degradation by MDM2, which serves as a *bona fide* E3 ligase mediating FOXO3a degradation. Moreover, the non-phosphorylated FOXO3a mutant (FOXO3a³ᴬ), which is resistant to MDM2-mediated degradation, exhibits potent inhibition of cell proliferation, induction of apoptosis and suppression of tumour growth. Our data demonstrate an essential role for ERK–MDM2-mediated FOXO3a regulation in tumorigenesis.
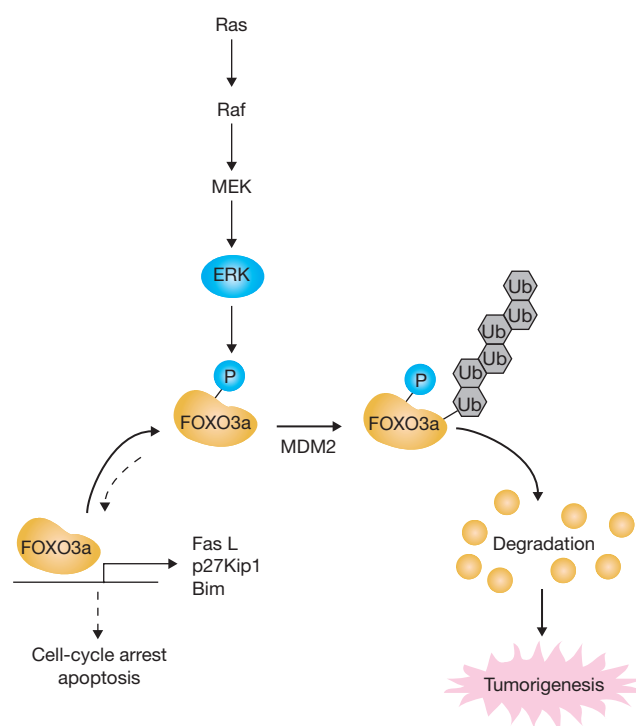

Figure 6 ERK promotes tumorigenesis by inhibiting FOXO3a via MDM2-mediated degradation. Schematic representation showing that ERK interacts with and phosphorylates FOXO3a at Ser 294, Ser 344 and Ser 425; phosphorylation at these residues increases FOXO3a-MDM2 interaction and enhances FOXO3a degradation through a MDM2-dependent ubiquitin-proteasome pathway, leading to tumorigenesis.

In addition, combining our observations and the results of previous studies, three important oncogenic kinases (AKT, IKKβ and ERK) are all involved in regulating FOXO3a nuclear localization and activity through discrete phosphorylation at different sites (see Supplementary Information, Fig. S4d)[17,30]. Thus, inactivation of FOXO3a may represent a critical and common step in survival pathways in cancer cells. Recently, ERK and p38 were shown to phosphorylate FOXO1. However, the functional outcomes were not discussed in the study[9]. On the other hand, overexpression of forkhead transcription factors (AFX and FKHR-L1) was shown to cause growth suppression in RASV12-transformed cells[34]. Consistently, our results show that maintaining FOXO3a activity by abolishing ERK-mediated phosphorylation is sufficient to revert cell growth caused by ERK activation due to RAS mutation (see Supplementary Information, Fig. S4a), which accounts for 30% of human cancers. In addition, expression of FOXO3a was shown to inhibit tumour development in animal models[17] (Fig. 5e), and repression of FOXO3a expression enhances tumour progression (Fig. 5g) and angiogenesis[10,17–19]. Taken together, the data suggest that enhancing FOXO3a activity may be a potential therapeutic strategy for treating human cancers.

ERK has been shown to promote cell growth and tumorigenesis[3,4,6,28]. ERK activation was also known to result in GSK3β inactivation and an accumulation of β-catenin in the nucleus[29], where β-catenin stimulates c-Myc and cyclin D1 transcription that, in turn, facilitate cell proliferation[29,35,36]. Thus, targeting RAS–ERK has been considered a promising approach for inhibition of tumour proliferation and to increase the sensitivity of cancer cells to chemotherapy[4,5]. Several pharmacological

reagents have been developed to specifically targeting RAF–MEK–ERK signalling, some of which have been approved for clinical use[4,5]. We propose that cancer cells acquire resistance to apoptosis and enhance cell proliferation through orchestrated inhibitions of FOXO3a and GSK3β with activated ERK, which further leads to constitutive survival signalling cascades and tumorigenesis. Furthermore, our study elucidates the possibility of increasing the therapeutic efficacy of ERK inhibitors by concurrent activation of FOXO3a. □

METHODS

Reagents and plasmids. MEK1 inhibitors U0126 and PD98059 were purchased from Cell Signaling. MG-132, CHX and EGF were purchased from Sigma. The dual-luciferase assay kit was purchased from Promega. GFP–FOXO3a construct was generated in our previous study[17]. Mutants of GFP–FOXO3a, GFP–FOXO3a[3A] and GFP–FOXO3a[3D], were generated using the Quick Change multi site-directed mutagenesis kit from Stratagene. MEK1[CA] and MDM2[464A] expression plasmids were gifts from P. P. Pandolfi (Harvard Medical School, Boston, MA) and D.-H. Yan (UTMDACC, Houston, TX). MDM2 and the MDM2 deletion mutant were from gifs from J. Chen (H. Lee Moffitt Cancer Center, Tampa, FL); the reporter plasmids p27–Luc and pGL2–6xDBE were gifts from T. Sakai (Kyoto Prefectual University of Medicine, Japan) and P. Coffer (University Medical Center, Utrecht, The Netherlands), and the pSuper–*FOXO3a* siRNA vector was a gift from A. Toker (Harvard Medical School, Boston, MA)[37].

Immunochemistry, *in vivo* ubiquitination and GST pulldown assays. Immunohistochemical staining, immunoblotting, immunoprecipitation and *in vivo* ubiquitination were performed, as previously described[25], with the following antibodies: FOXO3a, MDM2 (Santa Cruz Biotechnology), ERK (Upstate Biotechnology), p-ERK, p-serine (Cell Signaling), p27, p38, JNK1 (BD Biosciences) and Bim (Stressgen). For GST pulldown assays, GST–FOXO3a protein (10 µg) was incubated at 4 °C with 5 mg MCF-7 cell-extract overnight, and the GST-tagged proteins were recovered by incubating the reaction at 4 °C for 3 h with 20 µl glutathione–Sepharose 4B beads. The bead pellet was washed three times with 1 ml buffer (20 mM Tris–HCl at pH 7.5, 150 mM NaCl, 10% glycerol, 1% Triton X-100 and 2 mM EDTA). Boiled samples were then subjected to 8% SDS–PAGE.

Real-time PCR. Forward and reverse primer sequences were: *Bim*, 5′-AACCTTCTGATGTAAGTTCT-3′ and 5′-GTGATTGCCTTCAGGATTAC-3′; *p27*, 5′-GTGCGAGTGTCTAACGGGAG-3′ and 5′-GTTTGACGTCTTCTGAGGCC-3′; *FOXO3a*, 5′-GCTGTCTCCATGGACAATAG-3′ and 5′-GCTGGCTTGTTCTCTTGGAT-3.

In vitro kinase and *in vivo* ^{35}S-methionine labelling assays. Purified GST–FOXO3a protein was incubated with active ERK2 (Upstate Biotechnology) in the presence of 50 mM ATP in a kinase buffer containing 5 µCi γ-^{32}P-ATP for 30 min at 30 °C. Reaction products were resolved by SDS–PAGE, and products labelled with ^{32}P were visualized by autoradiography. The *in vivo* ^{35}S-methionine labelling was performed as previously described[25].

In-gel protein digestion. A slightly modified version of a previously published protocol was used[38]. Briefly, pieces of interest from the silver-stained gel were washed with 100 mM ammonium bicarbonate and ACN, reduced with DTT at 60 °C for 40 min and alkylated by IAA in the dark for 30 min. The gel pieces were washed twice with 50 µl 50% ACN and 50% 200 mM ammonium bicarbonate buffer (pH 8.0) for 5 min, dehydrated in 50 µl 100% ACN until the gel turned opaque white, and dried in a vacuum centrifuge for 30 min. The gel pieces were rehydrated in 5–10 µl 50 mM ammonium bicarbonate at 37 °C for 4 min. An equivalent volume (10–35 µl) of trypsin (Promega) solution (10 ng µl⁻¹ in 50 mM ammonium bicarbonate) was added until the gel pieces were fully immersed. After digestion at 30 °C overnight, the supernatants were transferred into new microtubules for IMAC purification.

Nanoelectrospray mass spectrometry. A nanoscale capillary LC-MS/MS analysis was performed by using an Ultimate capillary LC system (LC Packings) coupled to a QSTAR$_{XL}$ quadrupole (Q)–time-of-flight (TOF) mass spectrometer (Applied Biosystems), as previously described[39]. The nanoscale capillary LC separation was performed on an RP C18 column (15 cm × 75 m i.d.) with a flow rate of 200 nl min⁻¹ and a 70-minutelinear gradient of 5–50% buffer B. Buffer A contained 0.1% formic acid in 2% aqueous ACN, and buffer B contained 0.1% formic acid in 98% aqueous ACN. The nanoscale capillary LC tip used for online LC-MS was a PicoTip (FS360-20-10-D-20; New Objective). Data was acquired using an automatic information-dependent acquisition system (Applied Biosystems), which locates the most intense ions in a TOF MS spectrum and performs an optimized MS/MS analysis on the selected ions. The product ion spectra generated by nanoscale capillary LC-MS/MS were searched against National Center for Biotechnology Information databases for exact matches using the ProID (Applied Biosystems) and MASCOT search programs[40]. A *Homo sapiens* taxonomy restriction was used, and the mass tolerance of both precursor ions and fragment ions was set to ± 0.3 Da. Carbamidomethyl cysteine was set as a fixed modification, and serine, threonine and tyrosine phosphorylation were set as variable modifications. All phosphopeptides identified were confirmed by manual interpretation of the spectra.

CIP treatment. The cell lysate was harvested, followed by incubation with 1 µl 10 U µl⁻¹ CIP (New England Biolabs) in 50 µl CIP buffer for 1 h at 37 °C. Reactions were stopped by two washes in CIP buffer and boiling in gel-loading buffer.

Cell culture, cell growth, soft agar assay and FACS analysis. All cell cultures were kept in DMEM/F12 supplemented with 10% FBS at 5% CO_2 and the concentrations and time for each chemical treatment were as following: U0126 (5 µM, 4 h), PD98059 (20 µM, 4 h), MG-132 (20 µM, 6 h), CHX (1 µg ml⁻¹) and EGF (100 ng ml⁻¹). The cell growth rate was determined by MTT assay. Cells ($3 × 10^3$ per well) were plated in 96-well culture plates. After cells adhered, 20 µ MTT was added and incubated for 2 h before 100 µl lysis buffer (20% SDS in 50% *N,N*-dimethylformamide at pH 4.7) was added. After incubating, absorbance was measured at 570 nm. For the soft agar transformation assay, $5 × 10^4$ cells were placed in 1.5 ml DMEM with 10% FBS and 0.3% agarose and overlaid onto 3 ml DMEM with 10% FBS and 0.6% agarose in each well of a six-well plate. After 2–3 weeks, colonies larger than 2 mm in diameter were counted. For the FACS analysis, cells were trypsinized and fixed in 70% ice-cold ethanol overnight. Cells were then incubated with 1 ml propidium iodide solution (Sigma; 50 µg ml⁻¹ in PBS) plus 25 µg ml⁻¹ RNase for 30 min at 37 °C and measured.

Animal studies. Tumorigenesis assays were performed in an orthotopic breast cancer mouse model[41]. MDA-MB-435 breast cancer cells were transfected by liposome or electroporation (Amaxa Inc.). GFP-positive cells were selected by cell sorting. Cells ($2 × 10^6$) were injected into the mammary fat pads of nude mice ($n = 10$ per group). The remaining cells were used for soft agar assays and immunoblotting against FOXO3a, p27Kip1, Bim and caspase 3. Tumour size was measured weekly with a caliper, and tumour volume was determined using the formula: $l × w^2 × 0.52$, where l is the longest diameter and w is the shortest diameter.

Statistical analysis. SAS software (version 8.1) was used for statistical analysis (SAS Institute). A univariate analysis was used to determine the variable distributions. Categorical variables among the groups were compared with the χ-squared test or Fisher's exact test if 20% of the expected values were smaller than five. Continuous variables were analysed using the two-tailed Student's *t*-test. Linear regression analysis was used to analyse the FOXO3a and MDM2 expression in the lysates of breast cancer patients. A P value of <0.05 was considered statistically significant.

Note: Supplementary Information is available on the Nature Cell Biology website.

ARTICLES

1. Hanahan, D. & Weinberg, R. A. The hallmarks of cancer. *Cell* **100**, 57–70 (2000).
2. Vogelstein, B. & Kinzler, K. W. Cancer genes and the pathways they control. *Nature Med.* **10**, 789–799 (2004).
3. Yoon, S. & Seger, R. The extracellular signal-regulated kinase: multiple substrates regulate diverse cellular functions. *Growth Factors* **24**, 21–44 (2006).
4. Kolch, W. Coordinating ERK/MAPK signalling through scaffolds and inhibitors. *Nature Rev. Mol. Cell Biol.* **6**, 827–837 (2005).
5. Thompson, N. & Lyons, J. Recent progress in targeting the Raf/MEK/ERK pathway with inhibitors in cancer drug discovery. *Curr. Opin. Pharmacol.* **5**, 350–356 (2005).
6. Scholl, F. A., Dumesic, P. A. & Khavari, P. A. Effects of active MEK1 expression *in vivo*. *Cancer Lett.* **230**, 1–5 (2005).
7. Weinberg, R. A. Fas oncogenes and the molecular mechanisms of carcinogenesis. *Blood* **64**, 1143–1145 (1984).
8. Giehl, K. Oncogenic Ras in tumour progression and metastasis. *Biol. Chem.* **386**, 193–205 (2005).
9. Asada, S. *et al.* Mitogen-activated protein kinases, Erk and p38, phosphorylate and regulate Foxo1. *Cell Signal.* **19**, 519–527 (2006).
10. Greer, E. L. & Brunet, A. FOXO transcription factors at the interface between longevity and tumor suppression. *Oncogene* **24**, 7410–7425 (2005).
11. Finnberg, N. & El-Deiry, W. S. Activating FOXO3a, NF-kappaB and p53 by targeting IKKs: an effective multi-faceted targeting of the tumor-cell phenotype? *Cancer Biol. Ther.* **3**, 614–616 (2004).
12. Burgering, B. M. & Kops, G. J. Cell cycle and death control: long live Forkheads. *Trends Biochem. Sci.* **27**, 352–360 (2002).
13. Tran, H., Brunet, A., Griffith, E. C. & Greenberg, M. E. The many forks in FOXO's road. *Sci STKE* **RE5** (2003).
14. Dijkers, P. F. *et al.* Forkhead transcription factor FKHR-L1 modulates cytokine-dependent transcriptional regulation of p27(KIP1). *Mol. Cell Biol.* **20**, 9138–9148 (2000).
15. Schmidt, M. *et al.* Cell cycle inhibition by FoxO forkhead transcription factors involves downregulation of cyclin D. *Mol. Cell Biol.* **22**, 7842–7852 (2002).
16. Yang, J. Y., Xia, W. & Hu, M. C. Ionizing radiation activates expression of FOXO3a, Fas ligand, and Bim, and induces cell apoptosis. *Int. J. Oncol.* **29**, 643–648 (2006).
17. Hu, M. C. *et al.* IkappaB kinase promotes tumorigenesis through inhibition of forkhead FOXO3a. *Cell* **117**, 225–237 (2004).
18. Hu, M. C. & Hung, M. C. Role of IkappaB kinase in tumorigenesis. *Future Oncol.* **1**, 67–78 (2005).
19. Potente, M. *et al.* Involvement of Foxo transcription factors in angiogenesis and post-natal neovascularization. *J. Clin. Invest.* **115**, 2382–2392 (2005).
20. Paik, J. H. *et al.* FoxOs are lineage-restricted redundant tumor suppressors and regulate endothelial cell homeostasis. *Cell* **128**, 309–323 (2007).
21. Plas, D. R. & Thompson, C. B. Akt activation promotes degradation of tuberin and FOXO3a via the proteasome. *J. Biol. Chem.* **278**, 12361–12366 (2003).
22. Bond, G. L., Hu, W. & Levine, A. J. MDM2 is a central node in the p53 pathway: 12 years and counting. *Curr. Cancer Drug Targets* **5**, 3–8 (2005).
23. Zhou, B. P. *et al.* HER-2/neu induces p53 ubiquitination via Akt-mediated MDM2 phosphorylation. *Nature Cell Biol.* **3**, 973–982 (2001).
24. Uchida, C. *et al.* Enhanced Mdm2 activity inhibits pRB function via ubiquitin-dependent degradation. *EMBO J.* **24**, 160–169 (2005).
25. Yang, J. Y. *et al.* MDM2 promotes cell motility and invasiveness by regulating E-cadherin degradation. *Mol. Cell Biol.* **26**, 7269–7282 (2006).
26. Ries, S. *et al.* Opposing effects of Ras on p53: transcriptional activation of mdm2 and induction of p19ARF. *Cell* **103**, 321–330 (2000).
27. Phelps, M., Phillips, A., Darley, M. & Blaydes, J. P. MEK–ERK signaling controls Hdm2 oncoprotein expression by regulating *hdm2* mRNA export to the cytoplasm. *J. Biol. Chem.* **280**, 16651–16658 (2005).
28. Shaw, R. J. & Cantley, L. C. Ras, PI(3)K and mTOR signalling controls tumour cell growth. *Nature* **441**, 424–430 (2006).
29. Ding, Q. *et al.* Erk associates with and primes GSK-3β for its inactivation resulting in upregulation of β-catenin. *Mol. Cell* **19**, 159–170 (2005).
30. Brunet, A. *et al.* Akt promotes cell survival by phosphorylating and inhibiting a Forkhead transcription factor. *Cell* **96**, 857–868 (1999).
31. Honda, R. & Yasuda, H. Activity of MDM2, a ubiquitin ligase, toward p53 or itself is dependent on the RING finger domain of the ligase. *Oncogene* **19**, 1473–1476 (2000).
32. Honda, R. & Yasuda, H. Association of p19(ARF) with Mdm2 inhibits ubiquitin ligase activity of Mdm2 for tumor suppressor p53. *EMBO J.* **18**, 22–7 (1999).
33. Honda, R., Tanaka, H. & Yasuda, H. Oncoprotein MDM2 is a ubiquitin ligase E3 for tumor suppressor p53. *FEBS Lett.* **420**, 25–27 (1997).
34. Medema, R. H., Kops, G. J., Bos, J. L. & Burgering, B. M. AFX-like Forkhead transcription factors mediate cell-cycle regulation by Ras and PKB through p27kip1. *Nature* **404**, 782–787 (2000).
35. Lin, S. Y. *et al.* β-catenin, a novel prognostic marker for breast cancer: its roles in cyclin D1 expression and cancer progression. *Proc. Natl Acad. Sci. USA* **97**, 4262–4266 (2000).
36. Tetsu, O. & McCormick, F. β-catenin regulates expression of cyclin D1 in colon carcinoma cells. *Nature* **398**, 422–426 (1999).
37. Storz, P., Doppler, H. & Toker, A. Protein kinase D mediates mitochondrion-to-nucleus signaling and detoxification from mitochondrial reactive oxygen species. *Mol. Cell Biol.* **25**, 8520–8530 (2005).
38. Terry, D. E., Umstot, E. & Desiderio, D. M. Optimized sample-processing time and peptide recovery for the mass spectrometric analysis of protein digests. *J. Am. Soc. Mass Spectrom.* **15**, 784–794 (2004).
39. Lee, D. F. *et al.* IKKβ suppression of TSC1 links inflammation and tumor angiogenesis via the mTOR pathway. *Cell* **130**, 440–455 (2007).
40. Hirosawa, M., Hoshida, M., Ishikawa, M. & Toya, T. MASCOT: multiple alignment system for protein sequences based on three-way dynamic programming. *Comput. Appl. Biosci.* **9**, 161–167 (1993).
41. Chang, J. Y. *et al.* The tumor suppression activity of E1A in HER-2/neu-overexpressing breast cancer. *Oncogene* **14**, 561–568 (1997).
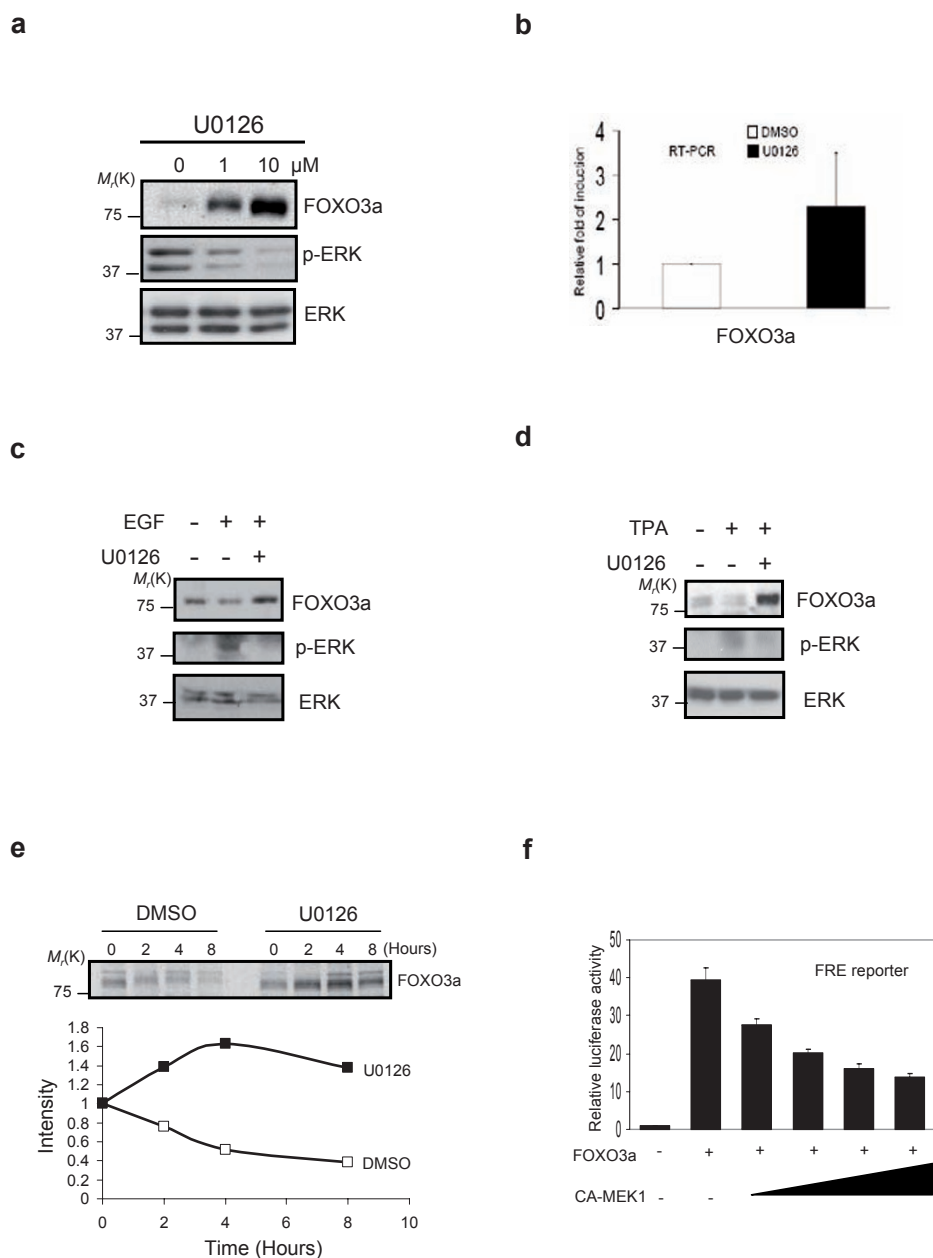
Figure S1 ERK inhibitor increased FOXO3a protein expression and activated ERK inhibited transcriptional activity of FOXO3a-responsive elements driven luciferase reporter. (**a**) Lysates of 293T cells were transfected with wild-type FOXO3a along with different dosages of U0126 and analyzed by immunoblotting. (**b**) Real time PCR transcript products of *FOXO3a* was measured, and the relative fold of induction was calculated and compared between DMSO and U0126 treated cells. (**c**) Serum starved MCF-7 cells were treated with EGF for 8 hrs with or without U0126. Cell lysates were subjected to immunoblotting with the antibodies indicated. (**d**) Serum starved MCF-7 cells were treated with 12-O-tetradecanoylphorbol 13-acetate (TPA) for 8 hrs with or without U0126. Cell lysates were subjected to immunoblotting with the antibodies indicated. (**e**) 293T cells were incubated with methionine and cysteine-free medium overnight. Cells were treated with or without U0126, pulsed with [^{35}S] Met for 30 minutes, and chased for the indicated time intervals. Cell lysates were immunoprecipitated with an anti-FOXO3a antibody and subjected to SDS-PAGE analyses. Gels were fixed, dried, and subjected to autoradiography (with an intensifying screen). (**f**) Lysates of 293T cells co-transfected with marked plasmids were subjected to luciferase assays with FOXO-responsive elements driven luciferase reporter. Graph shows the mean value of the representative results from three experiments (n=3) with s.d. conducted in duplicates for each. All the concentrations and time for treatment were described in the methods.
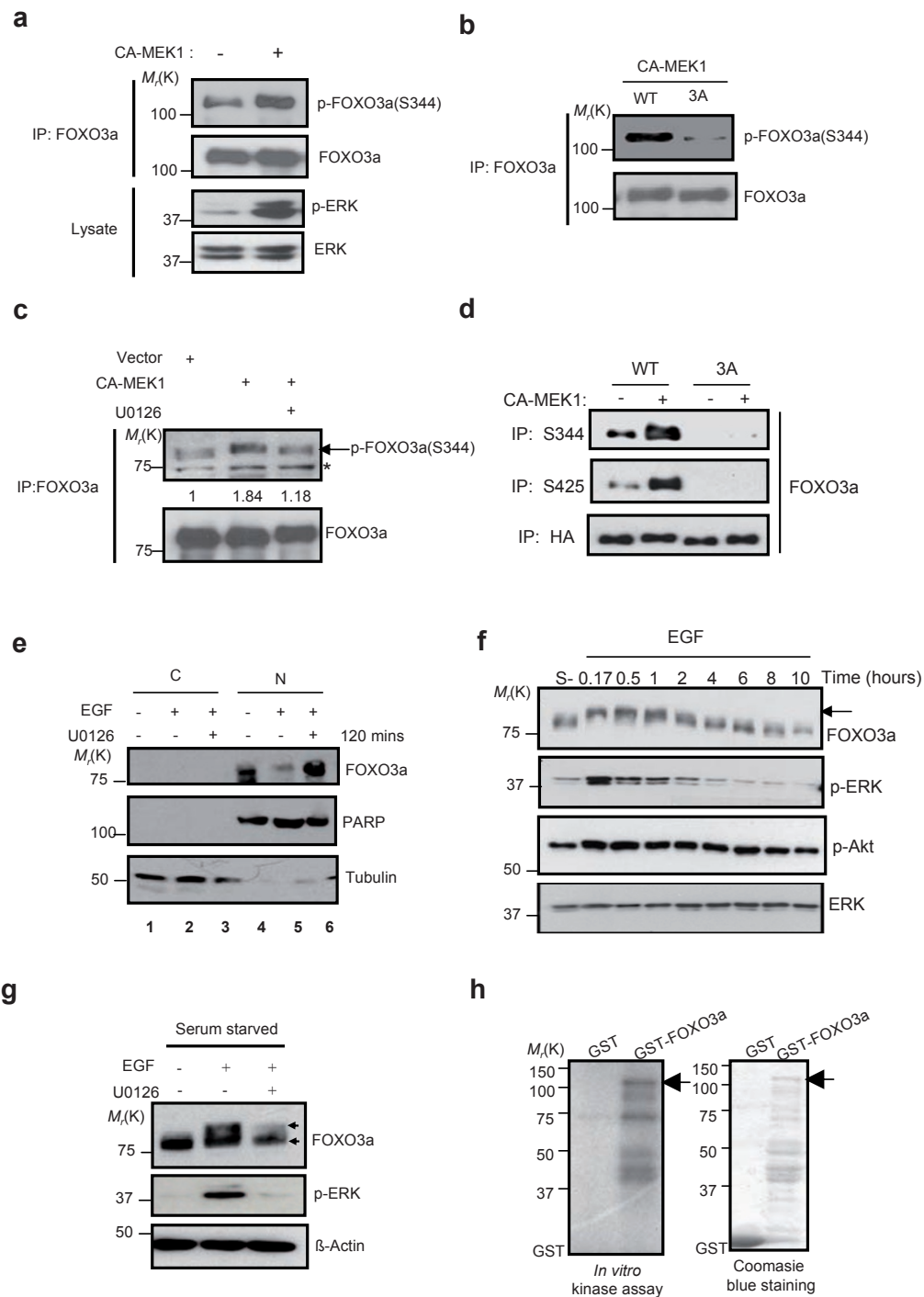
Figure S2 Identification of ERK phosphorylation sites of FOXO3a by specific phospho-antibody targeting p-FOXO3a (S294, S344 and S425).
(**a**) Lysates of 293T cells transfected FOXO3a with CA-MEK1 were subjected to immunoprecipitation and immunoblotting with the antibodies indicated. (**b**) Lysates of 293T cells co-transfected FOXO3a or FOXO3a-3A with CA-MEK1 were subjected to immunoprecipitation and immunoblotting (anti-FOXO3a and anti-p-FOXO3a-344). (**c**) Cells treated with PD98059 for 4 hours before the lysates were extracted and subjected to analysis as described in (a) (black arrow). The star represents a nonspecific band for P-FOXO3a antibody. (**d**) Lysates of 293 cells co-transfected with FOXO3a or FOXO3a-3A and CA-MEK1 were subjected to immunoprecipitation and immunoblotting

(IP: anti-p-FOXO3a-S344 or S425 and anti-HA; IB: anti-FOXO3a). (**e**) MCF-7 cells, after serum starvation, were treated with EGF for 120 minutes with or without U0126 then cytoplasmic and nuclear fractionations were analyzed by immunoblotting with indicated antibodies. (**f**) MCF-7 cells were extracted at the indicated times after serum starvation and EGF stimulation and then subjected to immunoblotting with the antibodies indicated. (**g**) The FOXO3a band upshift is blocked by ERK inhibitor U0126. MCF-7 cells were starved overnight and stimulated with EGF for 30 minutes. Lysates were left untreated or were treated with U0126 and subjected to immunoblotting. (**h**) ERK directly phosphorylates FOXO3a *in vitro*. *In vitro* kinase assay was performed by incubating recombinant activated ERK2 with full-length GST-FOXO3a.

a

b
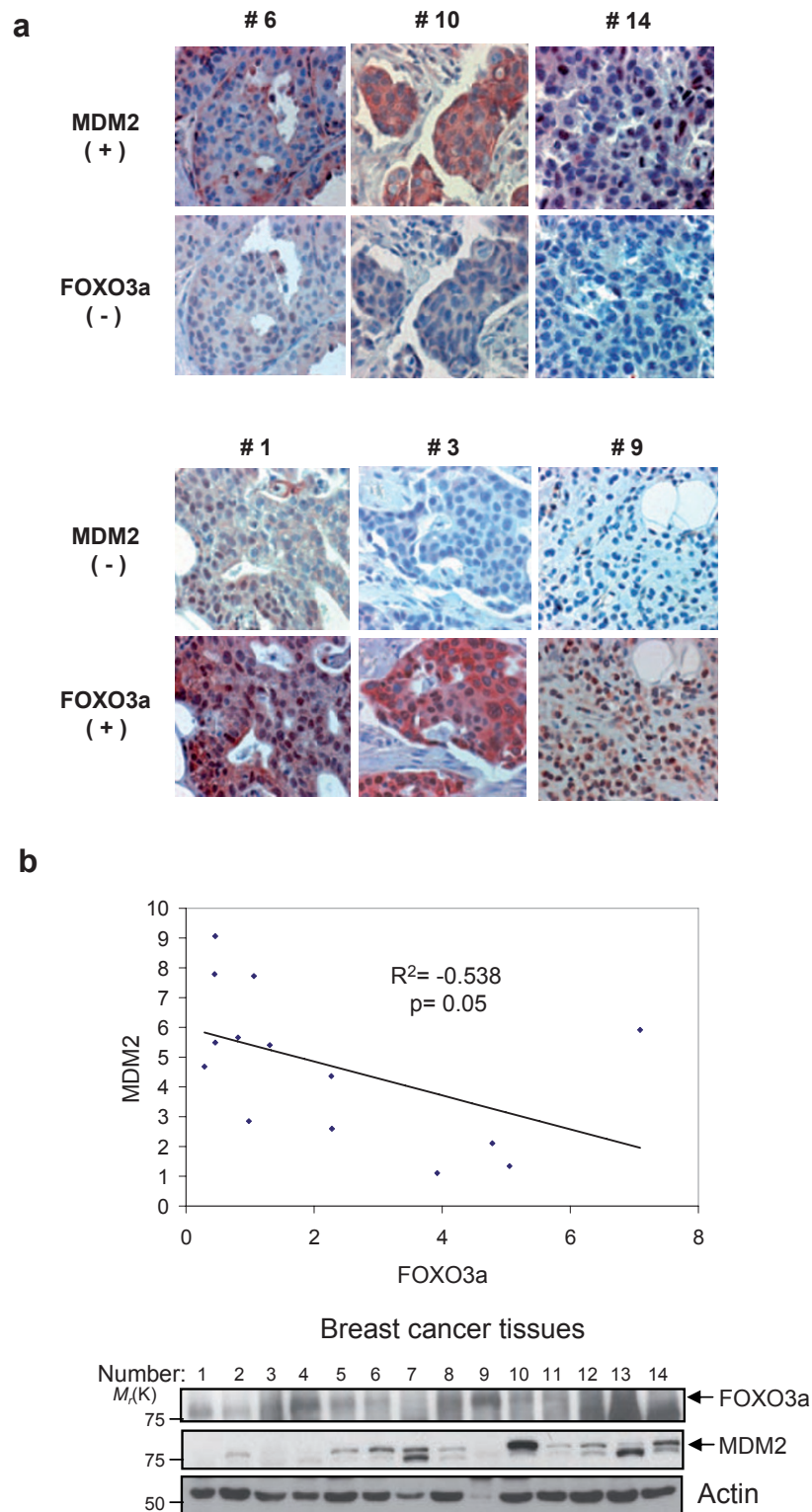
Figure S3 Inverse correlation of FOXO3a and MDM2 expression in human breast cancer patients. (**a**) The IHC levels of MDM2 and FOXO3a from consecutive tumor sections (# 6,10 and 14 represented MDM2+ and FOXO3a- ; # 1,3 and 9 represented MDM2- and FOXO3a+) of six patients. The patient numbers in (**a**) and (**b**) are the same. (**b**) Lysates from fourteen breast cancer patients were subjected to western blotting with indicated antibodies. The linear regression analysis was used to analyze the FOXO3a and MDM2 expression in the lysates of breast cancer patients.

Figure S4 (**a**) FOXO3a-3A mutant, but not FOXO3a-3D, inhibited cell growth. NIH-V12Ras cells were transfected with control vector, wild-type (WT) FOXO3a, and FOXO3a-3A and FOXO3a-3D mutants. After sorting with GFP marker for positive transfection, GFP-positive cells were subjected to MTT assay. Graph shows the mean value of the representative results from three experiments (n=3) conduc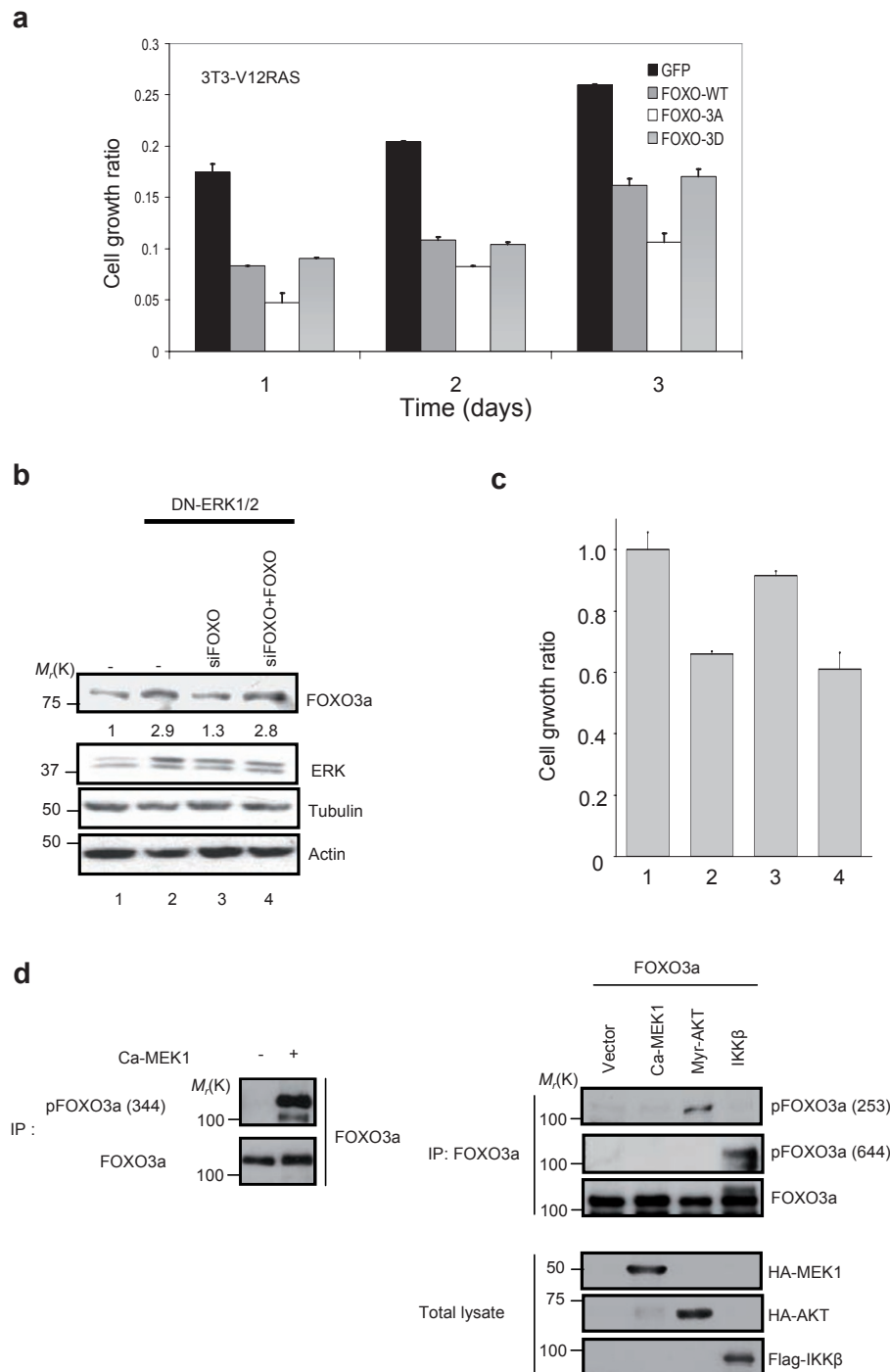ted in duplicates for each (s.d.) (**b**) (**c**) Forced expressing FOXO3a along with FOXO3a siRNA restores FOXO3a protein level as well as inhibits cell growth. MDA-MB-435 cells were transfected with control vector (lane 1), DN-ERK1 and DN-ERK2 (lane 2), DN-ERK1, DN-ERK2 and pSuper-FOXO3a siRNA (lane 3),

DN-ERK1, DN-ERK2 and pSuper-FOXO3a siRNA and FOXO3a (lane 4), and were subjected to (**b**) Western blot and (**c**) MTT assay. MTT assay (**c**) was performed using the same batch of transfected cells as (**b**) and labeled the same as shown in (**b**) Lane1 to lane 4. Graph shows the mean value of the representative results with s.d. from three experiments (n=3) conducted in duplicates for each. (**d**) Lysates of 293T cells co-transfected FOXO3a with CA-MEK1, Myr-AKT or IKKβ were immunoprecipitated with FOXO3a antibody and immunoblotted with the p-FOXO3a-S253, p-FOXO3a-S644 and total FOXO3a antibodies. Total lysates were separately by immnoblotted with indicated antibodies.
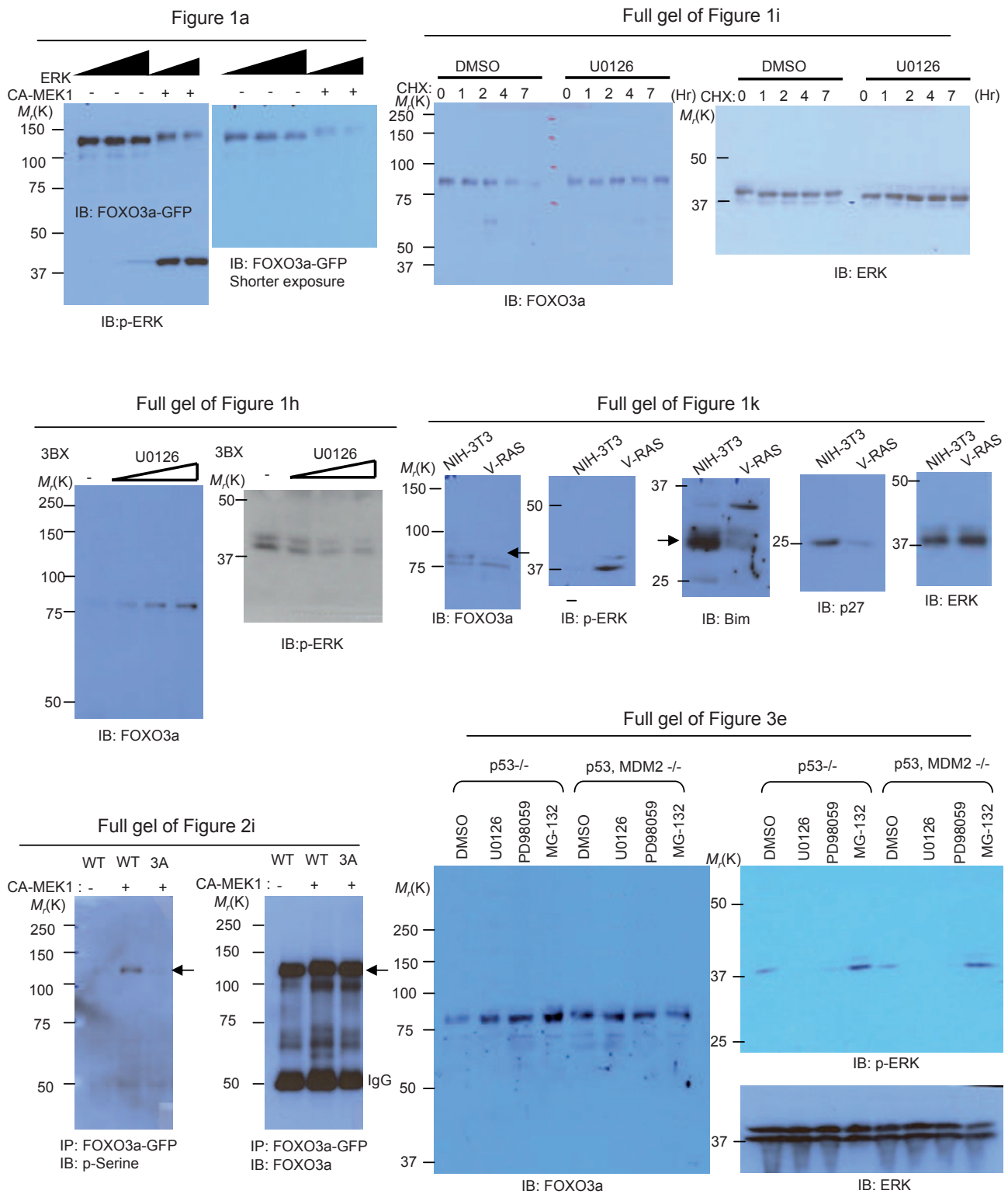
Figure 1a

ERK
CA-MEK1 : - - - + +   - - - + +

M_r(K)
150 —
100 —
75 —

IB: FOXO3a-GFP

50 —

37 —

IB: FOXO3a-GFP
Shorter exposure

IB:p-ERK

Full gel of Figure 1i

DMSO   U0126   DMSO   U0126

CHX: 0 1 2 4 7   0 1 2 4 7 (Hr)   CHX: 0 1 2 4 7   0 1 2 4 7 (Hr)
M_r(K) M_r(K)
250 —
150 —
100 —   50 —
75 —
                                     37 —
50 —
37 —

IB: FOXO3a   IB: ERK

Full gel of Figure 1h

3BX   U0126   3BX   U0126
  -                       -
M_r(K) M_r(K)
250 —   50 —
150 —   37 —
100 —
75 —   IB:p-ERK

50 —

IB: FOXO3a

Full gel of Figure 1k

M_r(K)
150 —
100 —
75 —

IB: FOXO3a   IB: p-ERK   IB: Bim   IB: p27   IB: ERK

NIH-3T3 V-RAS (for each panel)

50 —   37 —   37 —   50 —
37 —   25 —   25 —   37 —

Full gel of Figure 2i

WT WT 3A   WT WT 3A
CA-MEK1 : - + +   CA-MEK1 : - + +
M_r(K) M_r(K)
250 —   250 —
150 —   150 —
100 —   100 —
75 —   75 —
50 —   50 —   IgG

IP: FOXO3a-GFP   IP: FOXO3a-GFP
IB: p-Serine   IB: FOXO3a

Full gel of Figure 3e

p53-/-   p53, MDM2 -/-   p53-/-   p53, MDM2 -/-

DMSO U0126 PD98059 MG-132   DMSO U0126 PD98059 MG-132   DMSO U0126 PD98059 MG-132   DMSO U0126 PD98059 MG-132

M_r(K) M_r(K)
                                                50 —
250 —
                                                37 —
150 —
100 —   25 —
75 —
                                                IB: p-ERK
50 —

37 —   37 —

IB: FOXO3a   IB: ERK

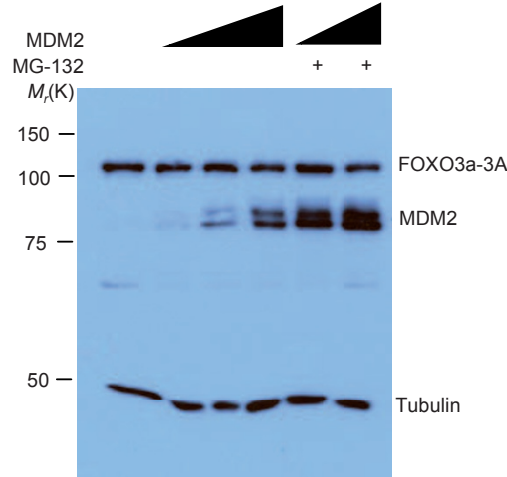**Figure S5** The full panels of primary gels from figures indicated.

Figure 4e

IB: FOXO3a-3D

IB: MDM2

IB: Tubulin

Figure 4f

IB: FOXO3a-3D

IB: MDM2-Δ9

IB: Tubulin
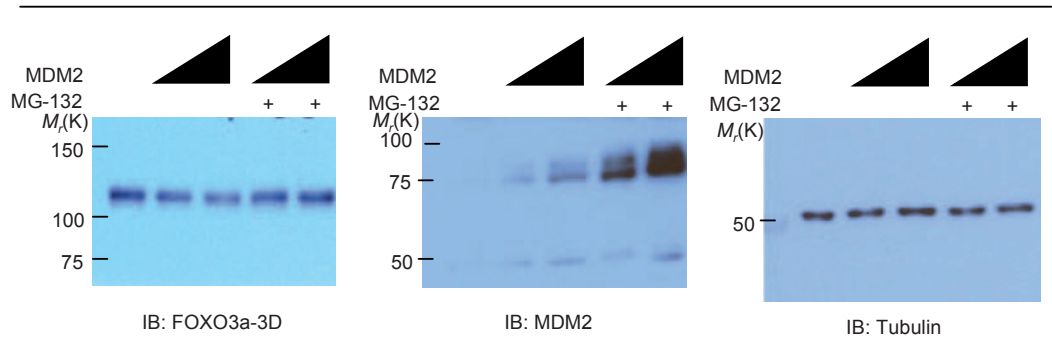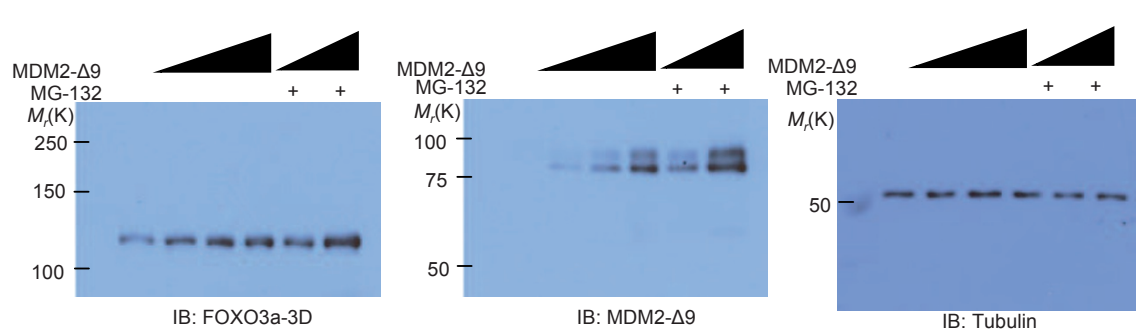
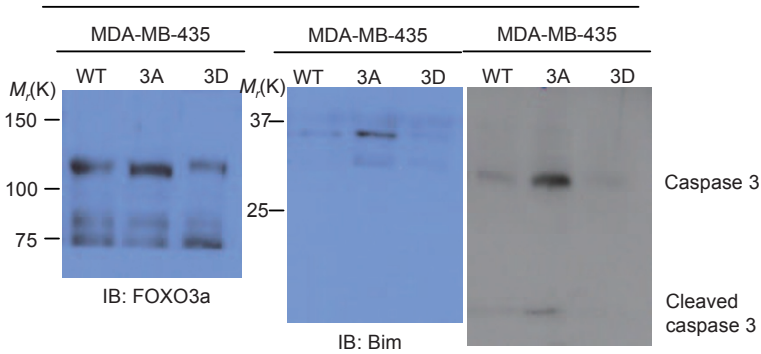## Figure 4g

Figure 5c

IB: FOXO3a

IB: Bim

Figure S6. The full panels of primary gels from figures indicated.